Modeling intra- and intermolecular correlations for linear and branched polymers using a modified test-chain self-consistent field theory

Renfeng Hu, David T. Wu, and Dapeng Wang

Phys. Rev. E **95**, 042502 — Published 13 April 2017

DOI: 10.1103/PhysRevE.95.042502

Modeling intra- and intermolecular correlations for linear and branched polymers using a modified test-chain self-consistent field theory

Renfeng Hu and David T. Wu*

Department of Chemical and Biological Engineering and Department of Chemistry, Colorado School of Mines, Golden, CO, 80401, USA

Dapeng Wang†

State Key Laboratory of Polymer Physics and Chemistry, Changchun Institute of Applied Chemistry, Chinese Academy of Sciences, Changchun, 130022, People's Republic of China

Abstract

A modified test-chain self-consistent field theory (SCFT) is presented to study the intra- and intermolecular correlations of linear and branched polymers in various solutions and melts. The key to the test-chain SCFT is to break the the translational symmetry by fixing a monomer at the origin of a coordinate. This theory successfully describes the crossover from self-avoiding walk at short distances, to screened random walk at long distances in a semi-dilute solution or melt. The calculations indicated that branching enhances the swelling of polymers in melts, and influences stretching at short distances. The test-chain SCFT calculations show good agreement with experiments and classic polymer theories. We highlight that the theory presented here provides a solution to interpret the polymer conformation and behavior in various conditions within the framework of one theory.

* dwu@mines.edu

† dapeng.wang@ciac.ac.cn

I. INTRODUCTION

The conformational properties of polymers are of renewed interest with the progress in synthesizing branched polymers with complex architectures[1–12]. Such novel synthesis can strictly control the number of branches and the polymerization degree, e.g., molecules of multiple armed star[4] and end-branched structures[5].

Conformations within a single polymer molecule can be strongly influenced by enthalpic interactions, steric repulsions and conformational entropy, particularly for polymers with a high number of arms emanating from one or multiple branching points. In this case, crowding can lead to stretching of arms near the branch points resulting in overall swelling of the polymer. The single molecule conformation can in turn influence how this molecule interacts with surrounding molecules. These intramolecular correlations influence interpenetration and miscibility in the case of blends, but can also be expected to influence entanglements and chain dynamics.

The characterization of the correlations in polymer homogeneous solutions and melts have been widely studied using scattering techniques[13–16]. In recent years small angle neutron scattering (SANS) has extended to polymer micelles, gel networks and inhomogeneous systems, e.g., copolymers in solution or in blends, and polymer blends containing novel nonlinear architectures[17]. In the interpretation of the SANS experiments, Gaussian chain conformations for melts are commonly assumed for branched polymers[16, 18–20], neglecting the possibility of swelling due to steric crowding.

The polymer conformation isn't always Gaussian. In semi-dilute polymer solutions in good solvent, the polymer conformations undergo a crossover from self-avoiding walk (SAW) to random walk statistics at a length scale corresponding to the blob size ξ[21, 22]. In the Daoud and Cotton[23] model for star polymers, the blob size increases with increasing distance from the core to the outside, behaving as an unswollen core and a swollen regime near the core, up to the concentration blob size ξ when the internal concentration matches the solution concentration.

Several molecular simulation studies have been carried out showing the swelling of nonlinear polymers. A molecular dynamics simulation performed by Grest *et al.*[24] indicated that the conformation of arms in a star polymer follows SAW. Recent Monte Carlo simulations[25–27] showed that the backbone of a highly branched comb stiffens and stretches as the side

branches become longer and more closely spaced in general agreement with scaling expectations. Yethiraj[28] performed Monte Carlo simulations for highly branched polymers, and concluded that increasing the number or the length of branches without changing the backbone length will increase the stiffness of backbone significantly, but increasing side-chain stiffness does not always increase the stiffness of the backbone. A simulation of star polymers in a good solvent[29] also showed that the intramolecular density distribution corresponds to SAW statistics for arm conformation. These excellent simulation works consistently demonstrated that the nonlinear structure can result in swelling and stretching of both polymer backbones and side branches due to crowding effects.

Theories of the conformation of polymer melts and blends have been widely developed. For long-chain polymers, coarse-grained descriptions of the conformations have been successful not only for polymers of varying architectures in the bulk, but also for polymers at interfaces[22, 30–35]. In particular for SCFT, the Gaussian chain model is extended to account for the influence of surrounding chains by a self-consistent mean field. SCFT has enjoyed wide success in explaining the compositional distributions of a wide variety of homogeneous and inhomogeneous polymers[36–39]. However, one drawback of conventional SCFT is that correlations between monomers are only accounted for by the mean field. For highly crowded branched polymers, the correlations become more significant, and it would be desirable to break through the limit of the conventional SCFT to account for such correlations, even in homogeneous systems.

A well-developed method in the study of polymeric bulk thermodynamics is the polymer reference interaction site model (PRISM) theory[40–45]. The PRISM theory solves the liquid polymer system by calculating an integral equation (the PRISM equation) to obtain the intermolecular correlation function. PRISM theory is a general method capable to solve polymeric systems regardless of architectures. Grayce *et al.*[43] performed PRISM calculations and found swelling of star polymers in both solutions and melts. The stretching of arms was found near the branch point because of the long range excluded volume effect crowding around the core region. Later, Patil *et al.*[46] studied star and comb polymer melts applying PRISM. Their results indicated that swelling was enhanced with more compact arms or branches. For a long branched comb with a small number of branches, packing and swelling behaved as if a linear chain of the same length of its backbone. However, by increasing number while shortening the length of branches, the intermolecular correlation

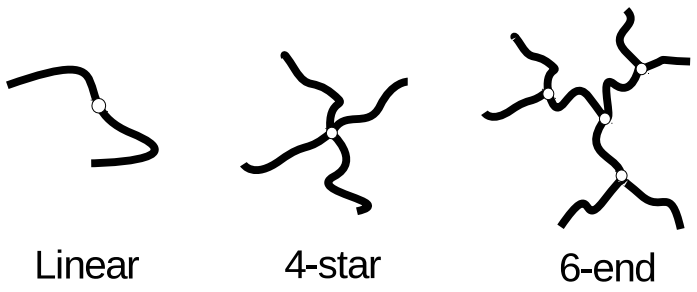

FIG. 1. Schematic illustration of linear and branched architectures[5].

of a highly branched comb was found to be significantly different from the linear chain, exhibiting an enhanced swelling similar to a star polymer melt.

In this paper, a test-chain self-consistent field theory algorithm is presented to study the conformations of linear and branched polymers in solutions and and melts. The SCFT is applied with an excluded volume potential and extends the theory to an algorithm capturing intra- and intermolecular correlations due to the steric and entropic driving force. Note that a similar but more restricted approach was implemented in a lattice model by Scheutjens and Fleers [47] for a homopolymer by fixing the joint of a star polymer as a grafted monomer at a boundary and calculating the intramolecular density profile in dilute solutions[48, 49]. The current study focuses on the swelling of linear and star-branched polymers with the scaling analysis for solutions and melts. The polymers tested are architecturally symmetric star and linear molecules shown in Fig. 1. We found that the branching can stretch the polymer at short distances from the core and result in overall swelling conformation of polymers in melts. The calculation of the modified SCFT showed good agreement with many experiments and computations.

II. THEORY AND FORMALISM

A. Scaling theory

Edwards [50] showed that in a semi-dilute solution, the monomers are screened by intermolecular interactions beyond the correlation length, $\xi_{\rm E} = \sqrt{12 v \rho_{\rm b}} b$, where b is the statistical segment length, $\rho_{\rm b}$ is the bulk density, and the excluded volume parameter v is positive for repulsive monomer interaction. De Gennes [22] commented that the Edwards correlation length does not reveal the swelling effect of polymers in solutions. The scaling theory for the intramolecular density distributions and the distance from one monomer of a SAW molecule is derived below. We focus on the scaling of the density profile and the excluded volume v. The symbol "$\cong$"in the derivation represents a full scaling expression with every variable, and the symbol $\sim$ denotes a scaling relation between two variables.

The scaling law of the monomer density distribution in a single linear chain as a function of distance from a given monomer can be written

$$\bar{\rho}(r) \cong c \bar{r}^{\alpha}, \tag{1}$$

where $\bar{\rho} = \rho(\bar{r}) b^3$ and $\bar{r} = r/b$ are dimensionless monomer density and distance, respectively. c is independent of $\bar{r}$ and the degree of polymerization N, but a function of the dimensionless excluded volume $\bar{v} = v b^{-3}$. The scaling exponent α depends on the single chain conformation. Particularly, $\alpha = -1$ for an ideal Gaussian chain, and $\alpha = -\frac{4}{3}$ for a swollen chain obeying SAW statistics, which is the Edwards' law[51]. The dimensionless size of the molecule, $\bar{R}$, scales as

$$\bar{R} \cong \bar{v}^{\beta} N^{\gamma}, \tag{2}$$

For a single chain with infinite dilute concentration that completely has SAW (i.e., $\alpha = -4/3$), $\beta = 1/5$ and $\gamma = 3/5$, respectively.

The integral of $\bar{\rho}(r)$ over the range of chain length scale $\bar{R}$ is the degree of polymerization, N of the chain:

$$N = \int_0^{\bar{R}} \bar{\rho}(\bar{r}) d\bar{r}^3 \cong \int_0^{\bar{R}} 4\pi c \bar{r}^{(\alpha+2)} d\bar{r}, \tag{3}$$

which gives

$$c \cong N \bar{R}^{-(\alpha+3)}, \tag{4}$$

where the dimensionless size of molecule $\bar{R}$ must satisfy

$$\bar{R} \cong (\bar{v})^{\beta} N^{\frac{1}{(\alpha+3)}} \tag{5}$$

to guarantee c is independent of N. Substitute eq 5 into eq 4 to obtain the general form of the dimensionless pre-factor c' as a function of v',

$$c \cong (\bar{v})^{-\beta(\alpha+3)}. \tag{6}$$

Therefore, eq 1 can be written as

$$\bar{\rho}(\bar{r}) \cong (\bar{v})^{-\beta(\alpha+3)} \bar{r}^{\alpha} \tag{7}$$

within the length scale of the molecule $\bar{R}$. Eq 7 shows the general scaling law for a single chain with finite excluded volume. For $\bar{v} \to 0$, the intramolecular density profile of the molecule is expected to be the Gaussian random walk. Otherwise eq 7 diverges.

The crossover from SAW to random walk occurs when the intermolecular density begins is equal to dimensionless bulk density $\bar{\rho}_{\mathrm{b}} = \rho_{\mathrm{b}} b^3$. The real chain correlation length $\bar{\xi}_{\mathrm{real}}$ is thus defined at where $\bar{\rho}(\xi) = \bar{\rho}_{\mathrm{b}}$. The general form of correlation length ξ can be written

$$\bar{\xi} \cong (\bar{v})^{\frac{\beta(\alpha+3)}{\alpha}} \bar{\rho}(\xi)^{\frac{1}{\alpha}}. \tag{8}$$

The screening length ξ_{real} for a Flory real chain is given as

$$\bar{\xi}_{\mathrm{real}} \cong (\bar{\rho}_{\mathrm{b}})^{-\frac{3}{4}} (\bar{v})^{-\frac{1}{4}} b, \tag{9}$$

and eq 6 reads

$$c \cong (\bar{v})^{-\frac{1}{3}}, \tag{10}$$

which is consistent with de Gennes' derivation[22].

B. The test-chain formalism

The general idea using SCFT to study the polymer bulk properties originated from the analytical single chain problem proposed by Edwards[50, 51], which involves one chain with a fixed end. The numerical solutions of SCFT basically followed the representation by Helfand for solving inhomogeneous polymer systems. A single chain consisting of N sites with unit Gaussian step length b is first considered. A density propagator called Green's function in a potential $\hat{W}$ observing site t position $\mathbf{r}$ and site t' at position $\mathbf{r}'$ can be defined as the path integral over all the polymer configurations:

$$G(\mathbf{r}, \mathbf{r}'; t, t') = \frac{\int \mathcal{D}\mathbf{R}(t) P(\mathbf{R}) \exp(-W(\mathbf{R})) \delta(\mathbf{R}(t) - \mathbf{r}) \delta(\mathbf{R}(t') - \mathbf{r}')}{\int \mathcal{D}\mathbf{R}(t) P(\mathbf{R}) \delta(\mathbf{R}(t) - \mathbf{r})}, \tag{11}$$

where $\mathbf{R}(t)$ is the configuration of the chain as a function of monomer index t. $P(\mathbf{R}(t))$ is the Gaussian statistics satisfying the Wiener distribution. (The energy unit of k_BT is chosen) For a chain labeled as α,

$$P(\mathbf{R}_\alpha(t)) \propto \exp\left[-\frac{3}{2b^2}\int_0^N dt \left|\frac{d\mathbf{R}_\alpha(t)}{dt}\right|^2\right], \tag{12}$$

and the compressible homogeneous interaction energy in terms of excluded volume effect $\hat{W}$ is given as a functional

$$\hat{W}[\hat{\rho}(\mathbf{r})] = \frac{v}{2}\int d\mathbf{r}\hat{\rho}(\mathbf{r})^2, \tag{13}$$

where $\hat{\rho}(\mathbf{r})$ is the microscopic density operator defined as

$$\hat{\rho}(\mathbf{r}) = \sum_{\alpha=1}^{n}\int_0^N dt\delta(\mathbf{r}-\mathbf{R}_\alpha(t)). \tag{14}$$

The canonical partition function of the system containing n chains is given by

$$\begin{aligned} Z &= \int \prod_{\alpha=1}^{n} \mathcal{D}\mathbf{R}_\alpha(t) P(\mathbf{R}_\alpha)\exp(-\hat{W}) \\ &= \mathcal{Z}_0 \int \mathcal{D}\rho\mathcal{D}\mu\, Q_0^n \exp\left[\frac{-v}{2}\int d\mathbf{r}\rho(\mathbf{r})^2 + \int d\mathbf{r}\mu(\mathbf{r})\rho(\mathbf{r})\right], \end{aligned} \tag{15}$$

where $\mathcal{Z}_0 = V^n/n!$ (V is the volume of the system). Q_0 is the single chain partition function in an external field μ. The free energy functional is

$$F[\rho,\mu] = \int d\mathbf{r}\left[\frac{v}{2}\rho(\mathbf{r})^2 - \mu(\mathbf{r})\rho(\mathbf{r})\right] - n\ln Q_0[\mu]. \tag{16}$$

Eq 15 can be written in terms of the Green's function defined by eq 11:

$$\begin{aligned} Z &= \iint d\mathbf{r}'d\mathbf{r}''G(\mathbf{r}',\mathbf{r}'';N,0) \\ &= \iiint d\mathbf{r}d\mathbf{r}'d\mathbf{r}''G(\mathbf{r}',\mathbf{r};t,0)G(\mathbf{r},\mathbf{r}'';N,t), \end{aligned} \tag{17}$$

The above integrals are simplified by defining the weight function

$$q(\mathbf{r};t) = \int d\mathbf{r}'G(\mathbf{r}',\mathbf{r};t,0) \tag{18}$$

and

$$q^\dagger(\mathbf{r};t) = \int d\mathbf{r}''G(\mathbf{r},\mathbf{r}'';N,t), \tag{19}$$

which represent the statistical weight for a chain of t sites starting at the origin to the chain end at $\mathbf{r}$ and the statistical weight of $N-t$ sites starting at $\mathbf{r}$ to the opposite direction, respectively.

The weight functions q and $q^\dagger$ satisfy the modified diffusion equation

$$\frac{\partial q(\mathbf{r})}{\partial t} = \frac{b^2}{6}\nabla^2 q(\mathbf{r}) - \mu(\mathbf{r})q(\mathbf{r}), \tag{20}$$

where $\mu(\mathbf{r}) = v\rho(\mathbf{r})$ is the self-consistent mean field potential by saddle-point approximation satisfying[36]:

$$\frac{\partial F[\rho,\mu]}{\partial \rho} = \frac{\partial F[\rho,\mu]}{\partial \mu} = 0. \tag{21}$$

The monomer density $\rho(\mathbf{r})$ is thus given by

$$\rho(\mathbf{r}) = -\frac{\partial \ln Q_0[\mu]}{\partial \mu}, \tag{22}$$

and it can be evaluated by

$$\rho(\mathbf{r}) = \mathcal{N}\frac{\int_0^N dt q(\mathbf{r};t)q^\dagger(\mathbf{r};t)}{\int_0^\infty d^3\mathbf{r} q(\mathbf{r};N)q^\dagger(\mathbf{r};N)}, \tag{23}$$

where $\mathcal{N}$ is the normalization constant. The integrand of the numerator is the unnormalized density distribution at $\mathbf{r}$. The denominator guarantees that the probability of finding one segment over the volume is 1.

The Laplacian in eq 20 is reduced to be radius r dependent only because of the spherical symmetry, which is given as

$$\frac{\partial q(r;t))}{\partial t} = \frac{b^2}{6}\left(\frac{\partial^2 q(r;t)}{\partial r^2} + \frac{2}{r}\frac{\partial q(r;t)}{\partial r}\right) - \mu(r)q(r;t), \tag{24}$$

with boundary conditions $q(r<0;t) = q^\dagger(r<0;t) = 0$ and $\frac{\partial q}{\partial r}|_{r_{\max}} = \frac{\partial q^\dagger}{\partial r}|_{r_{\max}} = 0$, where $r_{\max}$ represents the radius of the system.

Define $q^{\text{fix}}(r;t;t_{\text{fix}})$ and $q^{\dagger\text{fix}}(r;t;t_{\text{fix}})$ as the statistical weight functions of the molecule with a fixed site t_{fix}. The initial conditions are $q^{\text{fix}}(r;0;t_{\text{fix}}) = 1$ and $q^{\dagger\text{fix}}(r;N;t_{\text{fix}}) = 1$. However, when $t = t_{\text{fix}}$, the diffusion along monomers by eq 20 is reset to solve $q^{\text{fix}}(r;t > t_{\text{fix}};t_{\text{fix}})$ and $q^{\dagger\text{fix}}(r;t < t_{\text{fix}};t_{\text{fix}})$. The reset intitial conditions at t_{fix} must satisfy $q^{\text{fix}}(r;t = t_{\text{fix}};t_{\text{fix}}) = \delta(r)$ and $q^{\dagger\text{fix}}(r;t = t_{\text{fix}};t_{\text{fix}}) = \delta(r)$, respectively. Similarly, define $q^{\text{free}}(r;t;t_{\text{fix}})$ and $q^{\dagger\text{free}}(r;t;t_{\text{fix}})$ to represent the statistical weights of one of the free polymer around the fixed chain in the system. The initial conditions for the free molecule are $q^{\text{free}}(r;0;t_{\text{fix}}) = 1$ and $q^{\dagger\text{free}}(r;N;t_{\text{fix}}) = 1$.

In bulk polymers, considering multiple chains by fixing t_{fix} of one molecule, the complete SCF potential is therefore

$$\mu(r;t_{\text{fix}}) = v\left(\rho^{\text{fix}}(r;t_{\text{fix}}) + \rho^{\text{free}}(r;t_{\text{fix}})\right), \tag{25}$$

where ρ^{fix} is the intramolecular density of the chain selected to hold t_{fix} at the origin, and ρ^{free} is the density distribution of all free molecules The intramolecular monomer density distribution of the fixed chain from site t_{fix} is thus written as

$$\rho^{\text{fix}}(r;t_{\text{fix}}) = \frac{\int_0^N dt\ q^{\text{fix}}(r;t;t_{\text{fix}})q^{\dagger\text{fix}}(r;t;t_{\text{fix}})}{4\pi\int_0^{r_{\max}} dr\ q^{\text{fix}}(r;N;t_{\text{fix}})q^{\dagger\text{fix}}(r;N;t_{\text{fix}})r^2}, \tag{26}$$

and the intermolecular density $\rho^{\text{free}}(r;t_{\text{fix}})$ is

$$\rho^{\text{free}}(r;t_{\text{fix}}) = \frac{\rho_{\text{b}}V}{N}\frac{\int_0^N dt\ q^{\text{free}}(r;t;t_{\text{fix}})q^{\dagger\text{free}}(r;t;t_{\text{fix}})}{4\pi\int_0^{r_{\max}} dr\ q^{\text{free}}(r;N;t_{\text{fix}})q^{\dagger\text{free}}(r;N;t_{\text{fix}})r^2}, \tag{27}$$

where ρ_{b} is the bulk monomer density.

The calculation of the density propagators of a branched structure can be referenced by Fredrickson[37]. Taking a 3-arm structure labeling 1, 2, and 3 for each arm as an example. t_{fix} locates on arm 3. $q1(r;t;t_{\text{fix}})$ diffuses from the end of arm 1, and $q1^{\dagger}(r;t;t_{\text{fix}})$ diffuses towards the end of arm 1. $q2$ and $q3$ diffuses from the end of arm 2 and 3, respectively. At t_{joint}, $q1^{\dagger}(r;t_{\text{joint}};t_{\text{fix}})$ is given as $q1^{\dagger}(r;t_{\text{joint}};t_{\text{fix}}) = q2(r;t_{\text{joint}};t_{\text{fix}})q3(r;t_{\text{joint}};t_{\text{fix}})$. A brief illustration of propagating q and $q^{\dagger}$ is given in Fig. 2.

The SCF calculation iterates by solving eq 24, eq 25, eq 26 and eq 27, including two sets of modified diffusion equations to solve the fixed and free chain statistical weight functions. The segment length b is set to be 1 to keep the results in dimensionless units. The Crank-Nicolson algorithm is used to solve the differential equations, and the Picard algorithm is applied in SCF iteration by updating μ^i. A mixing ratio $\lambda = 0.05$ ($\lambda \in (0,1]$) is applied to update μ^i in terms of $\mu^i = (1-\lambda)\mu^{i-1} + \lambda v\rho^i(r)$. Minimize $\epsilon = \frac{\sum_j |\mu_j^i - \mu_j^{i-1}|}{\sum_j |\mu_j^i|}$ until satisfying the tolerance of the convergence $\epsilon_{\text{t}} < 10^{-7}$, where i is the index of the ith iteration and j is the index of the spatial grids.

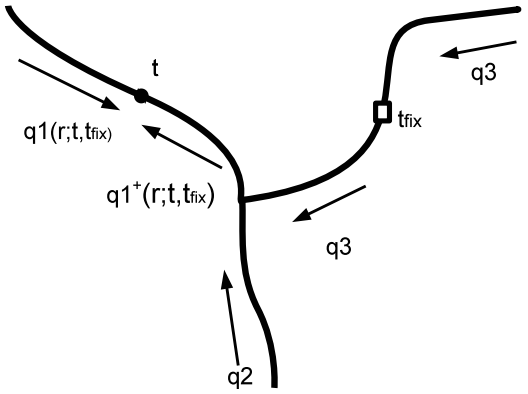

FIG. 2. Illustration to calculate the local density probability of a 3-arm structure. In this example, the molecule is fixed at $t_{\rm fix}$. As $q3$ is solved from the end of the chain and reaches $t_{\rm fix}$, $q3$ is reset to an initial condition, $q3(r; t = t_{\rm fix}; t_{\rm fix}) = \delta(r)$.

III. RESULTS AND DISCUSSION

A. Dilute solution of linear and star polymers

A single linear chain of $N = 50$ in a dilute solution is studied using test-chain SCFT. Eq 7 and eq 8 indicate that the molecular weight N does not influence the scaling of density and ξ. The resolution of the discretization grids is $\Delta r = 0.02b$ unless otherwise specified. The excluded volume parameter $\bar{v}$ ranges from 0 to 100. $\bar{v}$ is dependent of the compressibility[33]. In Fig. 3(a), the monomer density profiles show the real chain scaling of $-4/3$ if $\bar{v}$ is sufficiently large as a result of fixing the center of the molecule at the origin. The density profiles when $\bar{v} <\sim 0.1$ show less steep slopes, indicating that a weak excluded volume effect does not exhibit swelling. The plot for $\bar{v} = 0$ is very close to $\bar{v} = 0.01$ and indistinguishable from this scale, reflecting a Gaussian conformation with a slope close to 1. In the cases of $\bar{v} >\sim 1$, the density profiles indicate that the polymer conformation becomes swollen and the slope of the single chain density profile is very close to $-4/3$ within the range of the plot when $\bar{v} = 10$. Another feature of strong excluded volume is that the slope changes at a length scale of R, which is likely due to weaker correlations further from the center of mass. For $\bar{r} \to 0$, the molecule should be always SAW because the monomer with a finite excluded volume do not interact with other monomers. However, due to the finite grid size, this limit is not captured by the calculation. The density profiles from the held end monomer of the same

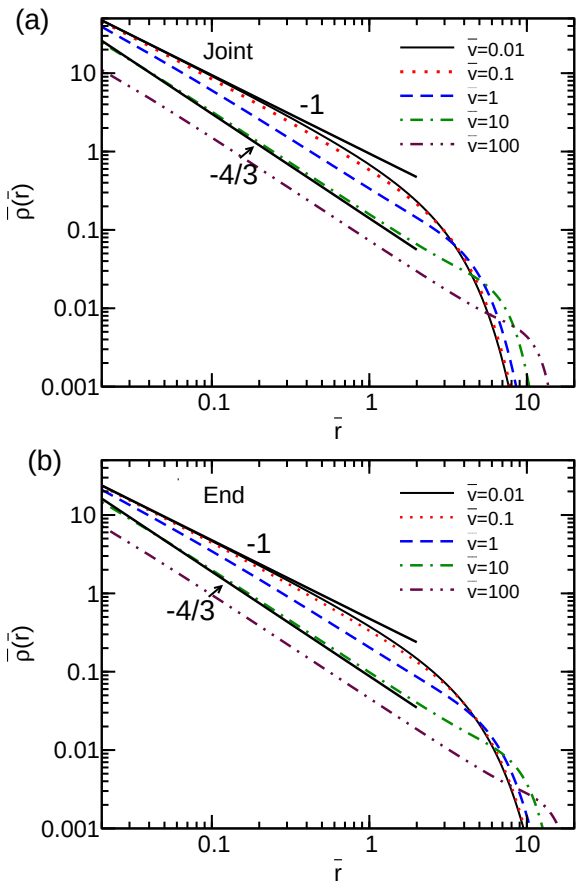

FIG. 3. The intramolecular density profiles of a linear single molecule for different values of excluded volume $\bar{v}$ in log-log scales. (a) The intramolecular density profiles of a linear molecule from the center. (b) The intramolecular density profiles of a linear molecule from the end. The length of the molecule $N = 50$.

linear chain is plotted in Fig. 3(b). The scaling exponent is analogous to that of holding the center. Its slope close to -4/3 indicates the swelling of the molecule in a dilute solution for $\bar{v} >\sim 10$, and a slope close to -1 for $\bar{v} <\sim 0.1$ indicates the Gaussian conformation. The magnitude of the density from the end monomer scales 1/2 compared to the density from the center (Fig. 3(a)) because the accumulative density from the end is only half of that from the center.

A further study of star molecules in dilute solutions is performed using a model of 4-star with the arm length, $N_{\rm arm} = 25$ and $N = 100$. Analogous results to the case of single linear molecule of the density profiles from the joint and the end are shown in Fig. 4(a) and b, respectively. For $\bar{v} = 0$, the density profile is also indistinguishable from the plot of $\bar{v} = 0.01$.

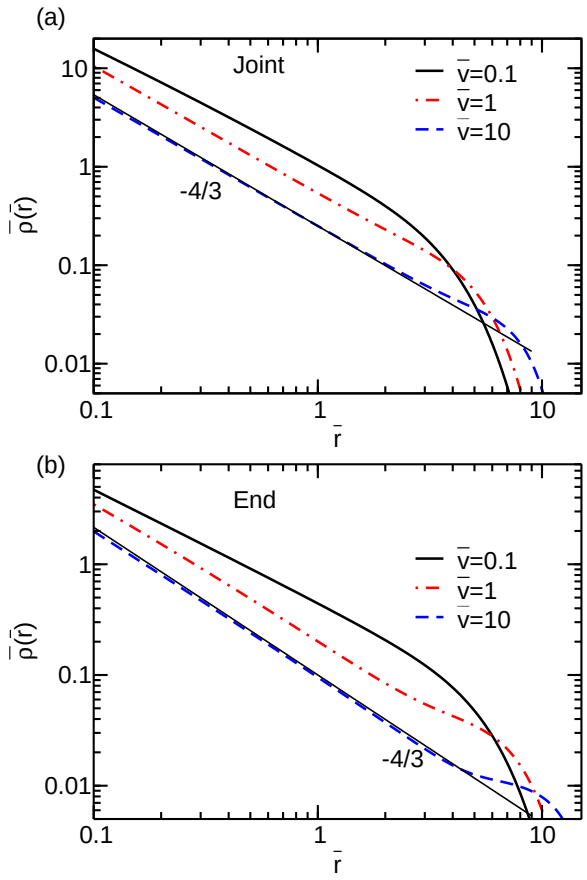

FIG. 4. The intramolecular density profiles of a 4-star polymer with $N_{\rm arm} = 25$ for different values of excluded volume $\bar{v}$ calculated from (a) the joint and (b) from the end.

The slope of $\rho(r)$ from the joint, similar to a linear molecule, implies that the conformation is similar to a SAW when $\bar{v} >\sim 1$. Fig. 4(b) shows that the molecule density from the held end behaves completely as a SAW when $\bar{v} = 10$ until the monomers are near the joint at a length scale of R. Thus, a small increase in density is present at long distances from the center. The scaling exponent of the SCFT agrees with the scaling theory for linear polymer solutions [22] and Monte Carlo simulations of star polymers demonstrated in Reference [29].

A series of f-stars with an identical arm length $N_{\rm arm} = 25$ were computed. The density distributions are shown in Fig. 5. The density profiles from the joint of f-star shown in Fig. 5(a) are similar to the profiles in the 4-star. The scaling exponent of the density profiles when $\bar{v} = 0.1$ is intermediate between -4/3 and -1, reflecting partially swollen. This indicates that the number of arm does not impact local swelling of a polymer in dilute

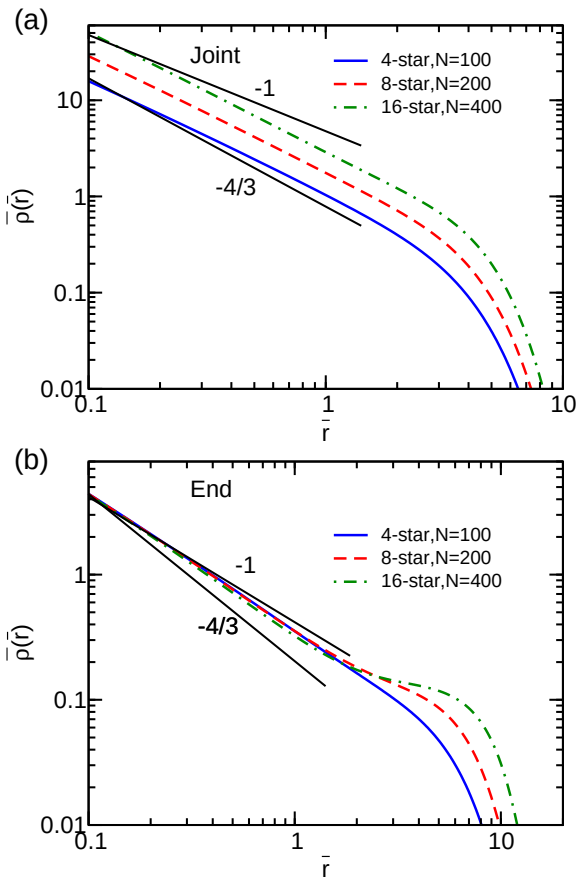

FIG. 5. Density distributions of f-star $N_{\rm arm} = 25$ and $\bar{v} = 0.1$ in a dilution solution condition calculating from (a) the joint and (b) the end, Respectively. $N_{\rm arm} = 25$, $N_{\rm star} = 100$.

solutions. However, the number of arm has a influence at long distances. For example, Fig. 5(b) shows the density profiles from the ends of polymer with increased number of arms. The scaling exponent of the density of the 16-star increases and then plateaus with a slope close to zero where the end monomer sees the accumulative density of the joint. This shows a good agreement with SANS results for the size of star polymers[52].

B. The end-to-end distance distribution

The end-to-end distance can be generated straightforwardly in the test-chain SCFT algorithm by holding one chain end fixed. In SCFT, the distributions of the distance between two ends can be written in terms of $q(r; N; 0)$, which is the statistical weight by holding the end 0 and diffuse to where the other end N. Thus, the three-dimensional normalized

end-to-end distance distribution is

$$P(r) = \frac{q(r;N;0)}{4\pi \int_0^\infty q(r;N;0) r^2 dr}. \tag{28}$$

The SCFT result reduces to an exact Gaussian chain without the mean field. If applying the excluded volume effect, the distribution function becomes a real chain type and is comparable with the des Cloizeaux's form[53]:

$$P(r) \cong \left(\frac{r}{\sqrt{\langle R^2\rangle}}\right)^{\sigma} \exp\left(-G\left(\frac{r}{\sqrt{\langle R^2\rangle}}\right)^{\tau}\right), \tag{29}$$

where the exponents and prefactors can be estimated[54, 55] as

$$P(r) \approx 0.278\langle R^2\rangle^{-3/2} \frac{r}{\sqrt{\langle R^2\rangle}}^{0.28} \exp\left(-1.206\left(\frac{r}{\sqrt{\langle R^2\rangle}}\right)^{2.43}\right) \tag{30}$$

for a Flory real chain. The mean square end-to-end distance $\langle R^2\rangle$ is given

$$\left\langle R^2\right\rangle = 4\pi \int_0^\infty P(r) r^4 dr. \tag{31}$$

Fig. 6 provides the SCFT results of the monomer end-to-end distribution profiles of the linear ($N = 100$) and 4-star ($N = 100$) molecule in dilute solutions. As shown in Fig. 6(a), by increasing $\bar{v}$, the linear chain becomes non-Gaussian and narrowly distributed. The des Cloizeaux plot is close to the SCFT plot with $\bar{v} = 1$. The end-to-end distribution profiles for strong repulsive polymers $\bar{v} >\sim 10$ show that the ends are distant close to$\sqrt{\langle R^2\rangle}$. However, the same calculation for a 4-star with $\bar{v} = 100$ in Fig. 6(b) shows that the end-end distribution is wider than a linear chain having the same degree of polymerization.

C. Semi-dilute solution and polymer melts

1. Density distribution functions

The test-chain SCFT can help understand the conformations of linear and non-linear polymers in a semi-dilute or concentrated solutions as well. As the density becomes finite, chains are screened due to intermolecular interactions. Eq 9 nicely captures a crossover in scaling exponent from self-avoiding to random walk, indicating that the intermolecular

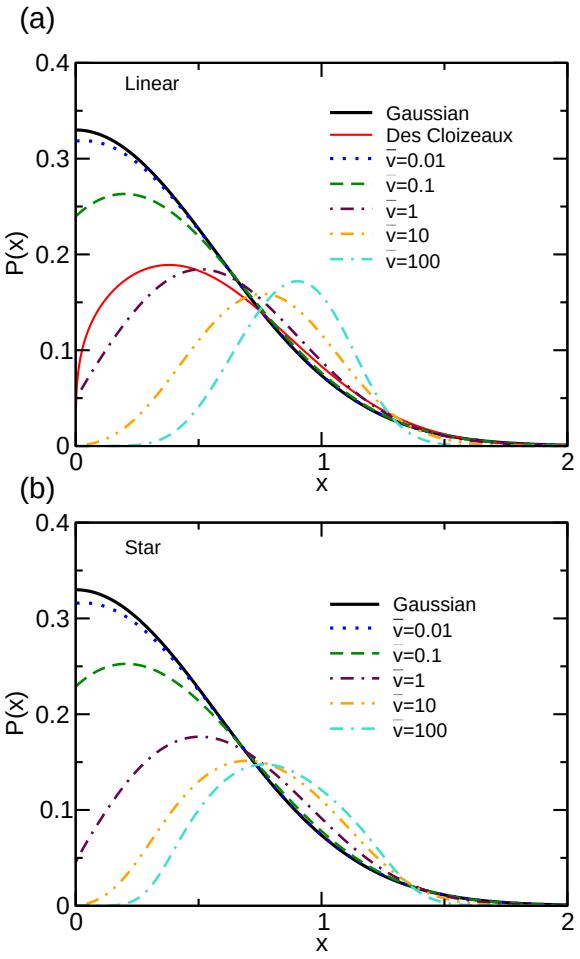

FIG. 6. The single chain end-to-end distribution function of (a) a linear molecule ($N = 50$) and (b) a 4-star ($N = 100$) by SCFT as a function of the reduced distance $x = \frac{r}{\sqrt{\langle R^2 \rangle}}$. The Gaussian model is provided as well for comparison.

interaction dominates at long distance.The SCFT calculations are performed in a linear solution with a finite density. The degree of polymerization of the linear molecule is $N = 50$ and the reduced average bulk monomer density $\bar{\rho}_{\rm b} = \rho_{\rm b} b^3$, which is defined by the total number of monomers over volume, is variable. The excluded volume parameter $\bar{v}$ is variable as well.

The intra- and intermolecular density profiles of linear polymers in semi-dilute solutions ($\bar{\rho}_{\rm b} = 0.2$) as a function of excluded volume parameters $\bar{v}$ from the joint and end are shown in Fig. 7. The intramolecular density profiles show different scaling exponents at the low $\bar{r}$ regime at approximately $\bar{r} <\sim 2$ in the figure. They cross over at $\bar{r} \approx 3$, and merge

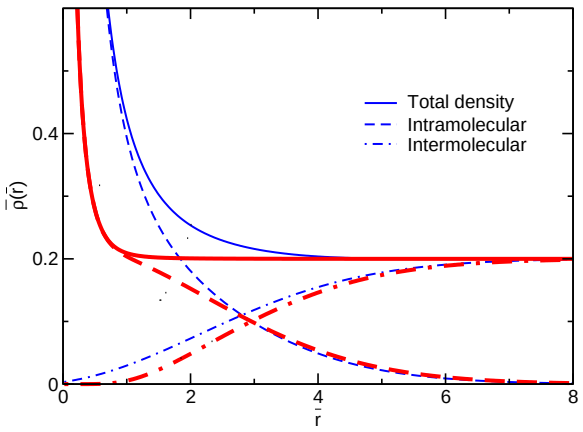

FIG. 7. Density profiles of a linear polymer with $N = 50$, and $\bar{\rho}_{\rm b} = 0.2$ in melts. The thin solid, dash and dash-dot lines correspond to the total, intra- and intermolecular density profiles when $\bar{v} = 1$, respectively. The thick solid, dash and dash-dot lines are the total, intra- and intermolecular density profiles with $\bar{v} = 100$, respectively.

at $\bar{r} >\sim 5$ in the range of the plot. A "correlation hole" is obtained on the plot of the intermolecular concentration profile. For $\bar{v} = 100$, less monomers approach to the short distance regime ($\bar{r} \approx 1$) for the strong repulsion due to monomer excluded volume.

Fig. 8(a) shows the intramolecular densities of a linear polymer with $N = 50$, $\bar{\rho}_{\rm b} = 0.2$ with varying excluded volumes. In homogeneous solutions, the overlap concentration is $c^* \cong N^{-4/5} b^{-3}$ for chains in SAW. The bulk density of $\bar{\rho}_{\rm b} = 0.2$ in Fig. 8(a) refers to a concentration above the limit of the semi-dilute solution because c^* is $\sim \mathcal{O}(10^{-2}) b^{-3}$. Again, the calculations show that the monomer density decreases as the strength of monomer exclusion $\bar{v}$ increases.

For solutions with small excluded volume (e.g., $\bar{v} < 0.01$), the molecule behaves as Gaussian random walk. This is the same as the single chain conformation in dilute solutions. Moreover, as increasing $\bar{v}$ from 0.01 to 1, a partially screened regime can be obtained(Fig. 8(a)). Although the complete SAW scaling exponent, $-4/3$, within the blob[22] is not captured by test-chain SCFT, the calculation is still expected to yeld SAW at $\bar{r} \to 0$. In the current resolution($\Delta\bar{r} = 0.02$), at short distances from the origin where $\bar{r} \approx 0.1$, the density profile has a transitional exponent between $-4/3$ and -1 and the profiles merge to Gaussian random walk exponent, -1, at long distances. However, the random walk regime is vanishing as $\bar{v}$ approaches 100. In particular, the intramolecular density profile of $\bar{v} = 100$

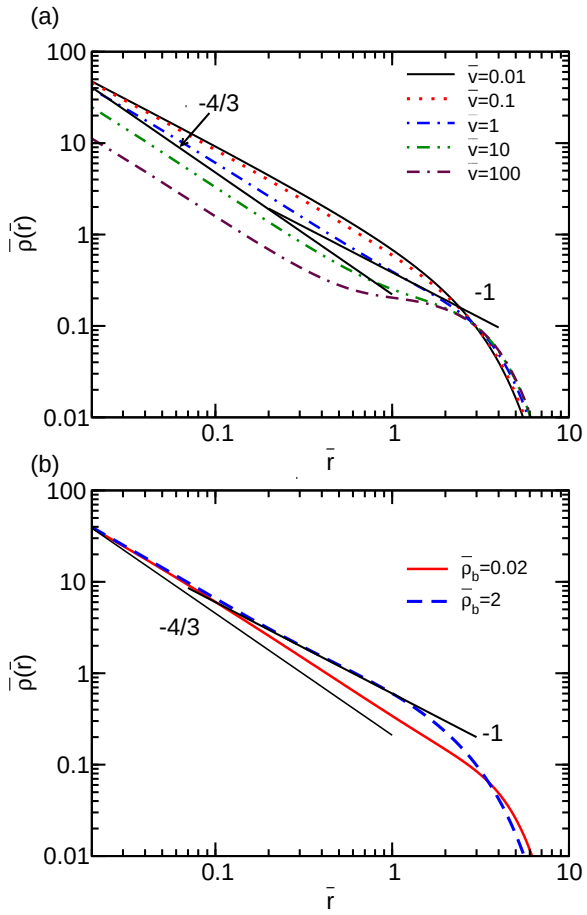

FIG. 8. The intramolecular density profiles for linear polymer in various solutions. (a) $\bar{\rho}_{\rm b} = 0.2$, $\bar{v}$ varies from 0.01 to 100. The slope of the density profile in the log-log scales is between $-4/3$ and -1 at $\bar{r} \approx 0.1$. (b) $\bar{v} = 1$, $\bar{\rho}_{\rm b}$ varies from 0.02 to 2.

does not show a random walk slope of -1 but a higher density in the bulk in the log-log scales. This is due to the strong repulsion among monomers. If the bulk concentration is increased while fixing the excluded volume, as is shown in Fig. 8(b), the screening of the molecules can therefore still be captured at a higher concentration. When $\bar{r}$ goes to zero, the intramolecular density profiles will merge together regardless of the value of the bulk densities.

2. The scaling analysis

In the section, we discussed the scaling of excluded volume in the intramolecular density profile at short distances, $\bar{\rho}(\bar{r}) \sim \bar{r}^{\alpha}\bar{v}^{-\beta(\alpha+3)}$. The plot of $\bar{\rho}(\bar{r})/\bar{r}^{\alpha}$ vs. $\bar{v}$ is shown in Fig. 9(a) at distances $\bar{r} < 0.1$. The bulk density keeps constant $\bar{\rho}_{\rm b} = 0.2$. When $\bar{v} \leqslant 0.01$, $\alpha = -1$; when $\bar{v} \geqslant 1$, $\alpha = -4/3$, according to the discussion of Fig. 8(a). In particular, two regimes for $\bar{\rho}(\bar{r})/\bar{r}^{\alpha}$ against $\bar{v}$ in log-log scales are identified. When $\bar{v} \leqslant 0.01$, $\bar{\rho}(\bar{r})/\bar{r}^{\alpha}$ is independent of $\bar{v}$. However, when $\bar{v} > 1$, the scaling relationship between the monomer density and distance shows that $\bar{\rho}(\bar{r})/\bar{r}^{\alpha} \sim (\bar{v})^{-1/3}$, which is consistent with eq 10 as a SAW chain. The two regimes cross over within the range of $0.01 < \bar{v} < 1$.

The scaling analysis based on expressions from eq 1 to eq 10 primarily assumes that at short distances, the intramolecular density profile in a melt is the same as it is in dilute solutions. This assumption is true at $\bar{r} \leqslant 0.1$ in the SCFT calculations above, because the total monomer density at short distances is dominated by the intramolecular density (Fig. 7). However, significant differences are seen at long distances in melts with strong excluded volumes when comparing Fig. 3(a) and Fig. 8(a). As shown in Fig. 9(b), we found that $\bar{\xi}$ also crosses over at approximately $\bar{v} = 1$ but the slope for $\bar{v} > 1$ is -1/8. This is only half of the expected scaling exponent, $\bar{\xi} \sim \bar{v}^{-1/4}$, according to eq 9. If applying the intramolecular density profiles in dilute solutions, which are the crossed points in Fig. 9(b), the plot of $\bar{\xi}$ against $\bar{v}$ shows the scaling exponent of $\bar{\xi} \sim \bar{v}^{-1/4}$. The inset in Fig. 9(b) shows the difference of the screening lengths determined from intramolecular density profiles in a dilute solution and a melt. From the inset figure, a difference in conformation is seen at the regime of $\bar{\rho}(r) \approx \bar{\rho}_{\rm b}$ between the dilute and semi-dilute solutions. In particular, the single chain must maintains SAW at $\bar{\xi}$, but the chain conformation of the semi-dilute solution with $\bar{\rho}_{\rm b} = 0.2$ becomes non-SAW at much shorter distances than $\bar{\xi}$. The existence of both SAW and Gaussian random walk within $\bar{\xi}$ by SCFT leads to a weaker scaling exponent, -1/8 than the scaling theory, $-1/4$. Moreover, the crossover from weak v dependence to strong v dependence in Fig. 9 is consistent with the expected criteria of observing SAW using the z parameter:

$$z = \frac{3}{2\pi}^{3/2} \frac{v}{b^3} N^{1/2} \approx \frac{v}{b^3} N^{1/2}, \tag{32}$$

where the actual excluded volume, $v \approx b^3$ is the limit of observing SAW with a given N.

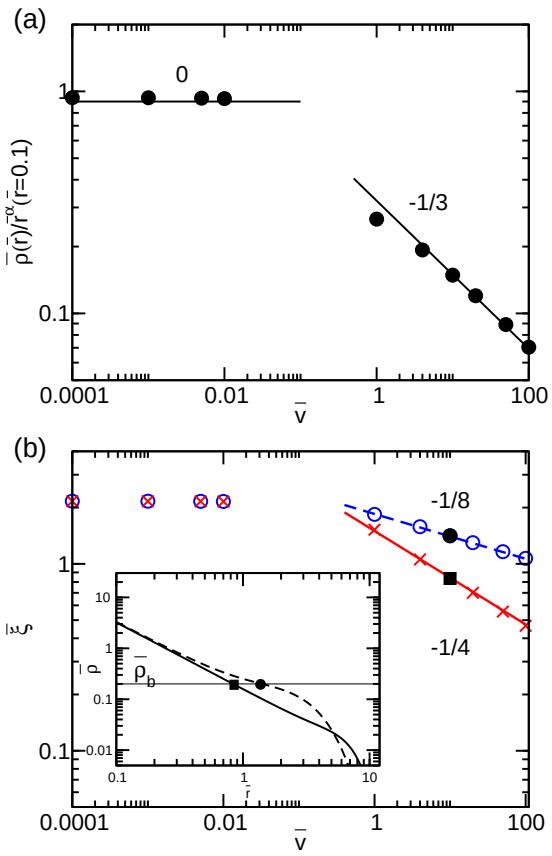

FIG. 9. Scaling analysis of the monomer density and correlation lengths against the excluded volume in concentrated solutions and melts of linear polymers. (a) The scaling dependence of scaled monomer density $\bar{\rho}(\bar{r})/\bar{r}^{\alpha}$ on excluded volume $\bar{v}$ at $\bar{r} = 0.1$ in solutions with $\bar{\rho}_{\rm b} = 0.2$ and $N = 50$. (b) The scaling dependence of correlation lengths $\bar{\xi}$ on $\bar{v}$ in solutions. The circles are obtained from the intramolecular densities of solutions in Fig. 8(a). Crossed points are obtained assuming that the intramolecular density profile in a melt is the same as the dilute solution (Fig. 3). The inset of (b) shows the way to obtain $\bar{\xi}$, where $\rho(\bar{\xi}) = \bar{\rho}_{\rm b}$, from the intramolecular density profiles. The dashed line: $\bar{v} = 10$, $\bar{\rho}_{\rm b} = 0.2$. The solid line: A dilute solution with $\bar{v} = 10$.

3. The swelling of star polymers in semi-dilute solutions and melts

Homogeneous melts composed of 4-star (N=100) molecules with different $\bar{\rho}_{\rm b}$, and $\bar{v}$, are studied. In general, the behavior of the star polymer conformation is found to be similar to that of the linear ones with N=50 (A linear is equivalent to a 2-star from the center as shown in Fig. 1). Fig. 10(a) and (b) compare the intramolecular density profiles by varying $\bar{v}$ and

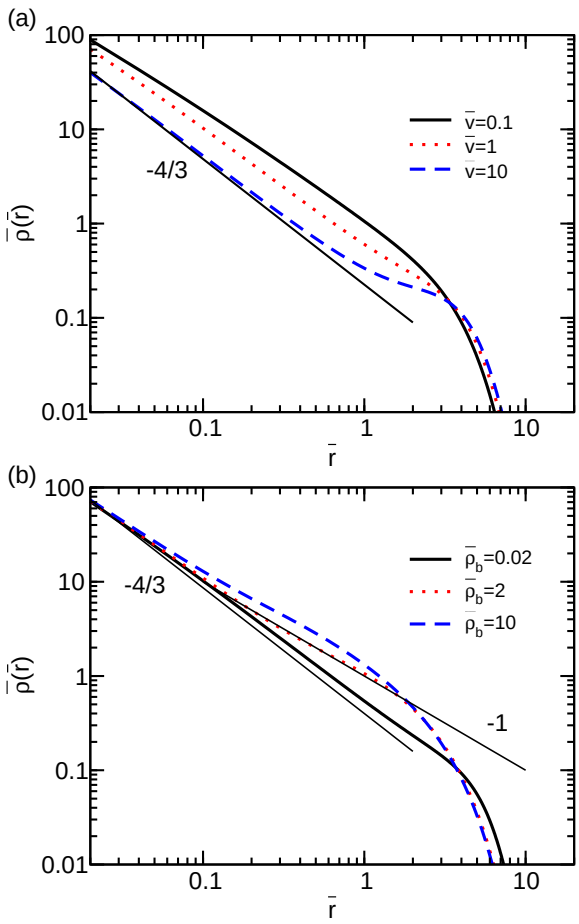

FIG. 10. The density profiles from the joint of 4-star chains with N = 100. (a) $\bar{\rho}_{\rm b} = 0.2$ and varying $\bar{v}$. (b) $\bar{v} = 1$ and varying $\bar{\rho}_{\rm b}$.

$\bar{\rho}_{\rm b}$, respectively. The density distribution of the 4-star melts are expected to merge to SAW at $\bar{r} \to 0$. For $\bar{v} < 10$, the observed exponents at short distances in the figure, $\bar{r} < 0.1$, are all less steep than that for $\bar{v} = 10$. Moreover, the distance where crossover occurs decreases as its density increases, as shown in Fig. 10(b). For instance, in the case of $\bar{\rho}_{\rm b} = 10$ and $\bar{v} = 1$, the polymers hardly show any SAW. On the contrary, the intramolecular density of the star solution with $\bar{\rho}_{\rm b} = 0.02$ is close to a dilute solution exhibiting an exponent close to SAW.

D. Structure factors of polymers in solutions and melts

The test-chain SCFT can be used to calculate the radial distribution function by holding every monomer each time and averaging by the degree of polymerization. The radial distribution for the intramolecular correlation, $\omega(r)$ and the intermolecular correlation, $g(r)$ of a polymer melt can be written directly as

$$\omega(r) = \frac{1}{N} \sum_{t_{\rm fix}=0}^{N} \rho^{\rm fix}(r; t_{\rm fix}) \tag{33}$$

and

$$g(r) = \frac{1}{N\rho_{\rm b}} \sum_{t_{\rm fix}=0}^{N} \rho^{\rm free}(r; t_{\rm fix}). \tag{34}$$

Given a polymer melt with $\rho_{\rm b}$ and the degree of polymerization N, the total structure factor is composed of both intra- and intermolecular contributions, which is

$$S(k) = \rho_{\rm b} N \omega(k) + \rho_{\rm b}^2 h(k), \tag{35}$$

where $\omega(k)$ is the intramolecular structure factor and $h(k)$ is the intermolecular contribution. $\omega(k)$ and $h(k)$ are three-dimensional Fourier transforms of pair correlation functions in spherical coordinate system, $\omega(r)$ and $h(r) = g(r) - 1$. The dimensionless structure factors are written as

$$\omega(\bar{k}) = 4\pi \int_0^\infty dr \frac{\bar{r}\sin(\bar{k}\bar{r})}{\bar{k}} \omega(\bar{r}), \tag{36}$$

and

$$h(\bar{k}) = 4\pi \int_0^\infty d\bar{r} \frac{\bar{r}\sin(\bar{k}\bar{r})}{\bar{k}} (g(\bar{r}) - 1), \tag{37}$$

where $\bar{k} = kb$.

$\omega(\bar{k})$ of the 4-star molecule of Gaussian, in a good dilute solution, in semi-dilute solution with $\bar{\rho}_{\rm b} = 0.2$ and in melts with $\bar{\rho}_{\rm b} = 10$, respectively, are shown in Fig. 11(a). In homogeneous melts, (e.g., $\bar{\rho}_{\rm b} = 10$), $\omega(\bar{k})$ is similar to the profile of a Gaussian chain. $\omega(\bar{k})$ in a semi-dilute solution is intermediate between the dilute solution and the ideal chain, reflecting a partially swollen conformation. In Fig. 11(b), the intermolecular structure factor $h(\bar{k})$ in four typical 4-star solutions are shown. In the case of $\bar{\rho}_{\rm b} = 10$, $h(\bar{k})$ is almost zero indicating the absence of intermolecular correlations in high density melts. Fig. 12 shows the total static structure factors of the 4-star molecules in different solutions. The peaks at

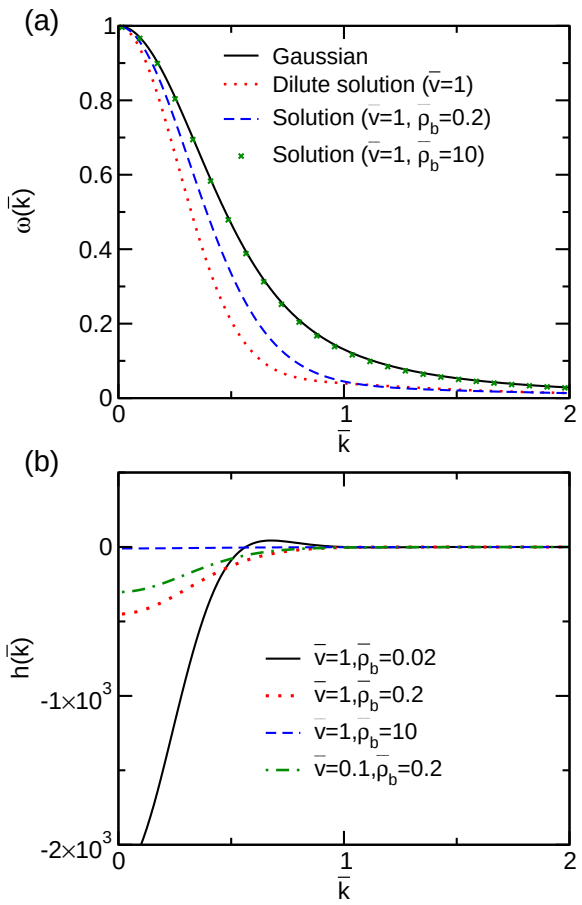

FIG. 11. The intramolecular $\omega(k)$ and intermolecular $h(k)$ structure factors of 4-star molecules ($N_{\rm star} = 100$). The Gaussian chain is also shown in (a) for comparison.

low $\bar{k}$ in the case of $\bar{v} = 1$ and $\bar{\rho}_b = 10$ correspond to melts with high bulk density and strong contribution of intermolecular structure factors, $\rho_{\rm b}^2 h(\bar{k})$. The result shows that a peak in $S(\bar{k})$ only depends on $\bar{\rho}_{\rm b}$ but not $\bar{v}$. This theoretical prediction has not been observed in SANS experiments for homogeneous polymer melts or blends, and remains an interesting question to explain the results of test-chain SCFT $S(k)$ at high density.

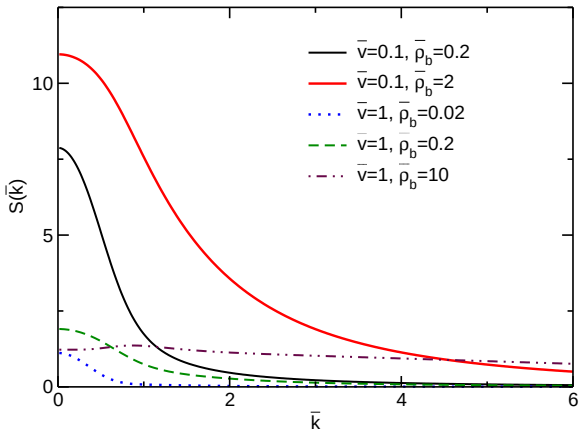

FIG. 12. Static structure factors of 4-star polymers with $N_{\text{star}} = 100$ in different solutions.

IV. CONCLUSION

A test-chain SCFT is presented to study polymer conformations of linear and branched polymers in various conditions. The results of linear polymers are in good agreement with classic polymer theory and simulation results[52, 56]. We summarized our finding as follows:

(1) The density profile of polymers from dilute solutions to melts, strongly depends on the excluded volume, $\bar{v}$. In dilute solutions, the conformation of a linear polymer is Gaussian when $\bar{v} < 0.1$. The conformation is smoothly swollen as increasing v. When $\bar{v} > 1$, the conformation can be identified as SAW. The conformation of branched polymers exhibit analogous behaviors.

(2) The calculations successfully captured a crossover regime from SAW to Gaussian in semi-dilute solutions and melts at a correlation length that decreases as $\bar{v}$ increases. The Gaussian regime is vanishing as $\bar{v}$ approaches 100. Moreover, the correlation length where the crossover occurs decreases as its density increases.

(3) Branching enhances the swelling of polymers in all conditions especially at regimes close to the branching point.

Finally, we emphasized that the test-chain theory is not only limited to any particular cases in this work. It is rather a universal means to modeling a broad variety of polymer systems[18, 57–61]. The algorithm presented here is to generalize a solution to model polymers with various architectures within the framework of one theory. This theory can be used to describe the polymer conformation and behaviors in many other complex environments

with a broad range of polymer concentrations[17, 60, 62–65].

V. ACKNOWLEDGMENTS

The research is funded by National Science Foundation (CBET-0731319). We gratefully acknowledge Prof. Mark Foster for fruitful discussions. Numerical computations are partially supported by Colorado School of Mines High Performance Computing Group. D. Wang thanks the support from the National "The Thousand Talents Plan" for Young Professionals.

---

[1] H. Hsieh and R. P. Quirk, *Anionic Polymerization: Principles and Practical Applications* (Marcel Dekker: New York, 1996).

[2] L. A. Archer and S. K. Varshney, Macromolecules **31**, 6348 (1998).

[3] T. D. Martter, M. D. Foster, T. Yoo, S. Xu, G. Lizzaraga, R. P. Quirk, and P. D. Butler, Macromolecules **35**, 9763 (2002).

[4] J. S. Lee, R. P. Quirk, M. D. Foster, K. M. Wollyung, and C. Wesdemiotis, Macromolecules **37**, 6385 (2004).

[5] J. S. Lee, R. P. Quirk, and M. D. Foster, Macromolecules **38**, 5381 (2005).

[6] M. G. McKee, S. Unal, G. L. Wilkes, and T. E. Long, Progress in Polymer Science **30**, 507 (2005).

[7] H. Gao and K. Matyjaszewski, Macromolecules **39**, 4960 (2006).

[8] Y. Chen, Z. Shen, E. Barriau, H. Kautz, and H. Frey, Biomacromolecules **7**, 919 (2006).

[9] J. Yoo, M. B. Runge, and N. B. Bowden, Polymer **52**, 2499 (2011).

[10] D. Wang, L. Pevzner, C. Li, K. Peneva, C. Y. Li, D. Y. C. Chan, K. Müllen, M. Mezger, K. Koynov, and H.-J. Butt, Phys. Rev. E **87**, 012403 (2013).

[11] S.-f. Wang, S. Yang, J. Lee, B. Akgun, D. T. Wu, and M. D. Foster, Phys. Rev. Lett. **111**, 068303 (2013).

[12] J. S. Lee, N.-H. Lee, S. Peri, M. D. Foster, C. F. Majkrzak, R. Hu, and D. T. Wu, Phys. Rev. Lett. **113**, 225702 (2014).

[13] W. Burchard, Advances in Polymer Science **48**, 1 (1983).

[14] A. T. Boothroyd, G. L. Squires, L. J. Fetters, A. R. Rennie, J. C. Horton, and A. M. B. G. De Vallera, Macromolecules **22**, 3130 (1989).

[15] B. Hammouda, R. M. Briber, and B. J. Bauer, Polymer **33**, 1785 (1992).

[16] B. Hammouda, Advances in Polymer Science **106**, 87 (1993).

[17] B. Hammouda, Polymer Reviews **50**, 14 (2010).

[18] J. S. Lee, M. D. Foster, and D. T. Wu, Macromolecules **39**, 5113 (2006).

[19] T. P. Russell, L. J. Fetters, J. C. Clark, B. J. Bauer, and C. C. Han, Macromolecules **23**, 654 (1990).

[20] C. C. Greenberg, M. D. Foster, C. M. Turner, S. Corona-Galvan, E. Cloutet, R. P. Quirk, P. D. Butler, and C. Hawker, Journal of Polymer Science Part B: Polymer Physics **39**, 2549 (2001).

[21] B. Farnoux, F. Boue, and J. Cotton, J. Phys. France **39**, 77 (1978).

[22] P. G. De Gennes, *Scaling Concepts in Polymer Physics*, 1st ed. (Cornell University Press: Ithaca, NY, 1979).

[23] M. Daoud and J. Cotton, J. Phys. France **43**, 531 (1982).

[24] G. S. Grest, K. Kremer, and T. A. Witten, Macromolecules **20**, 1376 (1987).

[25] Y. Rouault and O. V. Borisov, Macromolecules **29**, 2605 (1996).

[26] I. Carmesin and K. Kremer, Macromolecules **21**, 2819 (1988).

[27] H. P. Deutsch and K. Binder, The Journal of Chemical Physics **94**, 2294 (1991).

[28] A. Yethiraj, The Journal of Chemical Physics **125**, 204901 (2006).

[29] A. Di Cecca and J. J. Freire, Macromolecules **35**, 2851 (2002).

[30] E. Helfand and Y. Tagami, The Journal of Chemical Physics **57**, 1812 (1972).

[31] E. Helfand and Y. Tagami, The Journal of Chemical Physics **56**, 3592 (1972).

[32] D. G. Walton and A. M. Mayes, Phys. Rev. E **54**, 2811 (1996).

[33] D. T. Wu and G. H. Fredrickson, Macromolecules **29**, 7919 (1996).

[34] D. T. Wu, G. H. Fredrickson, and J.-P. Carton, The Journal of Chemical Physics **104**, 6387 (1996).

[35] G. J. Fleer, M. A. C. Stuart, J. M. H. M. Scheutjens, T. Cosgrove, and B. Vincent., *Polymers at interfaces* (Chapman and Hall: London, U.K., 1993).

[36] P. G. Ferreira and L. Leibler, The Journal of Chemical Physics **105**, 9362 (1996).

[37] G. Fredrickson, *The Equilibrium Theory of Inhomogeneous Polymers* (Oxford University Press: Oxford, U.K., 2006).

[38] M. W. Matsen, *Soft Matter*, edited by G. Gompper and M. Schick, Vol. 1 (Wiley-VCH Verlag GmbH & Co. KGaA: Weinheim, Germany, 2006).

[39] O. V. Rud, A. A. Polotsky, T. Gillich, O. V. Borisov, F. A. M. Leermakers, M. Textor, and T. M. Birshtein, Macromolecules **46**, 4651 (2013).

[40] J. G. Curro and K. S. Schweizer, Macromolecules **20**, 1928 (1987).

[41] K. Schweizer and J. Curro, Advances in Polymer Science **116**, 319 (1994).

[42] C. J. Grayce, A. Yethiraj, and K. S. Schweizer, The Journal of Chemical Physics **100**, 6857 (1994).

[43] C. J. Grayce and K. S. Schweizer, Macromolecules **28**, 7461 (1995).

[44] D. G. Gromov and J. J. de Pablo, The Journal of Chemical Physics **103**, 8247 (1995).

[45] A. Yethiraj, The Journal of Chemical Physics **108**, 1184 (1998).

[46] R. Patil, K. S. Schweizer, and T.-M. Chang, Macromolecules **36**, 2544 (2003).

[47] J. M. H. M. Scheutjens and G. J. Fleer, The Journal of Physical Chemistry **83**, 1619 (1979).

[48] J. Klein Wolterink, F. A. M. Leermakers, G. J. Fleer, L. K. Koopal, E. B. Zhulina, and O. V. Borisov, Macromolecules **32**, 2365 (1999).

[49] J. Klein Wolterink, J. van Male, M. A. Cohen Stuart, L. K. Koopal, E. B. Zhulina, and O. V. Borisov, Macromolecules **35**, 9176 (2002).

[50] S. F. Edwards, Proceedings of the Physical Society **88**, 265 (1966).

[51] S. F. Edwards, Proceedings of the Physical Society **85**, 613 (1965).

[52] L. R. Hutchings, R. W. Richards, S. W. Reynolds, and R. L. Thompson, Macromolecules **34**, 5571 (2001).

[53] J. des Cloizeaux, Phys. Rev. A **10**, 1665 (1974).

[54] M. Bishop, J. H. R. Clarke, A. Rey, and J. J. Freire, The Journal of Chemical Physics **95**, 4589 (1991).

[55] S. Caracciolo, M. S. Causo, and A. Pelissetto, The Journal of Chemical Physics **112**, 7693 (2000).

[56] J. C. Horton, G. L. Squires, A. T. Boothroyd, L. J. Fetters, A. R. Rennie, C. J. Glinka, and R. A. Robinson, Macromolecules **22**, 681 (1989).

[57] D. Wang, Y. Yuan, Y. Mardiyati, C. Bubeck, and K. Koynov, Macromolecules **46**, 6217 (2013).

[58] J. S. S. Wong, L. Hong, S. C. Bae, and S. Granick, Macromolecules **44**, 3073 (2011).

[59] C. Gerstl, G. J. Schneider, W. Pyckhout-Hintzen, J. Allgaier, S. Willbold, D. Hofmann, U. Disko, H. Frielinghaus, and D. Richter, Macromolecules **44**, 6077 (2011).

[60] B. McCulloch, V. Ho, M. Hoarfrost, C. Stanley, C. Do, W. T. Heller, and R. A. Segalman, Macromolecules **46**, 1899 (2013).

[61] D. Wang, R. Hu, J. N. Mabry, B. Miao, D. T. Wu, K. Koynov, and D. K. Schwartz, Journal of the American Chemical Society **137**, 12312 (2015).

[62] T. G. Desai, P. Keblinski, S. K. Kumar, and S. Granick, The Journal of Chemical Physics **124**, 084904 (2006).

[63] T. G. Desai, P. Keblinski, S. K. Kumar, and S. Granick, Phys. Rev. Lett. **98**, 218301 (2007).

[64] D. Mukherji, C. M. Marques, and K. Kremer, Nat Commun **5**, 4882 (2014).

[65] A. Chremos, E. Glynos, and P. F. Green, The Journal of Chemical Physics **142**, 044901 (2015).